# 3. Widths and Profiles of Spectral Lines

Spectral lines in discrete absorption or emission spectra are never strictly monochromatic. Even with the very high resolution of interferometers, one observes a spectral distribution $I(\nu)$ of the absorbed or emitted intensity around the central frequency $\nu_0 = (E_i - E_k)/h$ corresponding to a molecular transition with the energy difference $\Delta E = E_i - E_k$ between upper and lower levels. The function $I(\nu)$ in the vicinity of $\nu_0$ is called the *line profile* (Fig. 3.1). The frequency interval $\delta\nu = |\nu_2 - \nu_1|$ between the two frequencies $\nu_1$ and $\nu_2$ for which $I(\nu_1) = I(\nu_2) = I(\nu_0)/2$ is the *full-width at half-maximum* of the line (FWHM), often shortened to the *linewidth* or *halfwidth* of the spectral line.

The halfwidth is sometimes written in terms of the angular frequency $\omega = 2\pi\nu$ with $\delta\omega = 2\pi\delta\nu$, or in terms of the wavelength $\lambda$ (in units of nm or Å) with $\delta\lambda = |\lambda_1 - \lambda_2|$. From $\lambda = c/\nu$, it follows that

$$\delta\lambda = -(c/\nu^2)\delta\nu \,. \tag{3.1}$$

The *relative* halfwidths, however, are the same in all three schemes:

$$\left|\frac{\delta\nu}{\nu}\right| = \left|\frac{\delta\omega}{\omega}\right| = \left|\frac{\delta\lambda}{\lambda}\right| \,. \tag{3.2}$$

The spectral region within the halfwidth is called the *kernel of the line*, the regions outside ($\nu < \nu_1$ and $\nu > \nu_2$) are the *line wings*.

In the following sections we discuss various origins of the finite linewidth. Several examples illustrate the order of magnitude of different line-broadening effects in different spectral regions and their importance for high-resolution

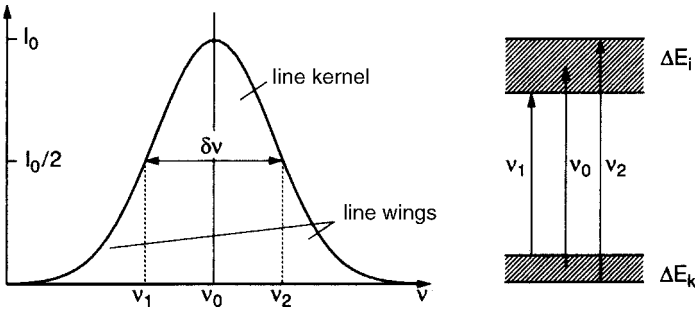


**Fig. 3.1.** Line profile, halfwidth, kernel, and wings of a spectral line

spectroscopy [3.1–3.4]. Following the usual convention we shall often use the angular frequency $\omega = 2\pi\nu$ to avoid factors of $2\pi$ in the equations.

## 3.1 Natural Linewidth

An excited atom can emit its excitation energy as spontaneous radiation (Sect. 2.7). In order to investigate the spectral distribution of this spontaneous emission on a transition $E_i \rightarrow E_k$, we shall describe the excited *atomic electron* by the classical model of a damped harmonic oscillator with frequency $\omega$, mass $m$, and restoring force constant $k$. The radiative energy loss results in a damping of the oscillation described by the damping constant $\gamma$. We shall see, however, that for real atoms the damping is extremely small, which means that $\gamma \ll \omega$ .

The amplitude $x(t)$ of the oscillation can be obtained by solving the differential equation of motion

$$\ddot{x} + \gamma\dot{x} + \omega_0^2 x = 0\,, \tag{3.3}$$

where $\omega_0^2 = k/m$.

The real solution of (3.3) with the initial values $x(0) = x_0$ and $\dot{x}(0) = 0$ is

$$x(t) = x_0\,\mathrm{e}^{-(\gamma/2)t}[\cos\omega t + (\gamma/2\omega)\sin\omega t]\,. \tag{3.4}$$

The frequency $\omega = (\omega_0^2 - \gamma^2/4)^{1/2}$ of the damped oscillation is slightly lower than the frequency $\omega_0$ of the undamped case. However, for small damping ($\gamma \ll \omega_0$) we can set $\omega \simeq \omega_0$ and also may neglect the second term in (3.4). With this approximation, which is still very accurate for real atoms, we obtain the solution of (3.3) as

$$x(t) = x_0\,\mathrm{e}^{-(\gamma/2)t}\cos\omega_0 t\,. \tag{3.5}$$

The frequency $\omega_0 = 2\pi\nu_0$ of the oscillator corresponds to the central frequency $\omega_{ik} = (E_i - E_k)/\hbar$ of an atomic transition $E_i \rightarrow E_k$.

### 3.1.1 Lorentzian Line Profile of the Emitted Radiation

Because the amplitude $x(t)$ of the oscillation decreases gradually, the frequency of the emitted radiation is no longer monochromatic as it would be for an oscillation with constant amplitude. Instead, it shows a frequency distribution related to the function $x(t)$ in (3.5) by a Fourier transformation (Fig. 3.2).

The damped oscillation $x(t)$ can be described as a superposition of monochromatic oscillations $\exp(\mathrm{i}\omega t)$ with slightly different frequencies $\omega$ and amplitudes $A(\omega)$

$$x(t) = \frac{1}{2\sqrt{2\pi}}\int_0^\infty A(\omega)\,\mathrm{e}^{\mathrm{i}\omega t}\,\mathrm{d}\omega\,. \tag{3.6}$$

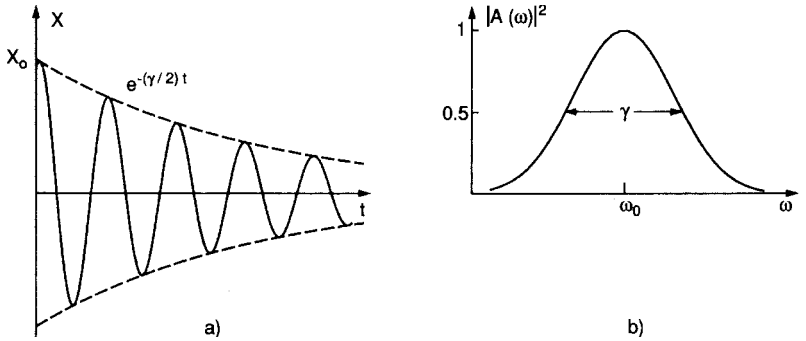


**Fig. 3.2.** (**a**) Damped oscillation: (**b**) the frequency distribution $A(\omega)$ of the amplitudes obtained by the Fourier transform of $x(t)$ yields the intensity profile $I(\omega-\omega_0) \propto |A(\omega)|^2$

The amplitudes $A(\omega)$ are calculated from (3.5) and (3.6) as the Fourier transform

$$A(\omega) = \frac{1}{\sqrt{2\pi}} \int_{-\infty}^{+\infty} x(t)\, \mathrm{e}^{-\mathrm{i}\omega t}\, \mathrm{d}t = \frac{1}{\sqrt{2\pi}} \int_{0}^{\infty} x_0\, \mathrm{e}^{-(\gamma/2)t} \cos(\omega_0 t)\, \mathrm{e}^{-\mathrm{i}\omega t}\, \mathrm{d}t \,. \tag{3.7}$$

The lower integration limit is taken to be zero because $x(t) = 0$ for $t < 0$. Equation (3.7) can readily be integrated to give the complex amplitudes

$$A(\omega) = \frac{x_0}{\sqrt{8\pi}} \left( \frac{1}{\mathrm{i}(\omega-\omega_0)+\gamma/2} + \frac{1}{\mathrm{i}(\omega+\omega_0)+\gamma/2} \right) . \tag{3.8}$$

The real intensity $I(\omega) \propto A(\omega)A^*(\omega)$ contains terms with $(\omega-\omega_0)$ and $(\omega+\omega_0)$ in the denominator. In the vicinity of the central frequency $\omega_0$ of an atomic transition where $(\omega-\omega_0)^2 \ll \omega_0^2$, the terms with $(\omega+\omega_0)$ can be neglected and the intensity profile of the spectral line becomes

$$I(\omega-\omega_0) = \frac{C}{(\omega-\omega_0)^2 + (\gamma/2)^2} \,. \tag{3.9}$$

The constant $C$ can be defined in two different ways:
For comparison of different line profiles it is useful to define a normalized intensity profile $L(\omega-\omega_0) = I(\omega-\omega_0)/I_0$ with $I_0 = \int I(\omega)\,\mathrm{d}\omega$ such that

$$\int_{0}^{\infty} L(\omega-\omega_0)\,\mathrm{d}\omega = \int_{-\infty}^{+\infty} L(\omega-\omega_0)\,\mathrm{d}(\omega-\omega_0) = 1 \,.$$

With this normalization, the integration of (3.9) yields $C = I_0\gamma/2\pi$.

$$\boxed{L(\omega-\omega_0) = \frac{\gamma/2\pi}{(\omega-\omega_0)^2+(\gamma/2)^2}\,,} \tag{3.10}$$

is called the *normalized Lorentzian profile*. Its full halfwidth at half-maximum (FWHM) is

$$\delta\omega_n = \gamma \quad \text{or} \quad \delta\nu_n = \gamma/2\pi\,. \tag{3.11}$$

Any intensity distribution with a Lorentzian profile is then

$$I(\omega-\omega_0) = I_0\frac{\gamma/2\pi}{(\omega-\omega_0)^2+(\gamma/2)^2} = I_0 L(\omega-\omega_0)\,, \tag{3.10a}$$

with a peak intensity $I(\omega_0) = 2I_0/(\pi\gamma)$.

**Note:** Often in the literature the normalization of (3.9) is chosen in such a way that $I(\omega_0) = I_0$; furthermore, the full halfwidth is denoted by $2\Gamma$. In this notation the line profile of a transition $|k\rangle \leftarrow |i\rangle$ is

$$I(\omega) = I_0 g(\omega-\omega_{ik}) \quad \text{with} \quad I_0 = I(\omega_0)\,,$$

and

$$g(\omega-\omega_{ik}) = \frac{\Gamma^2}{(\omega_{ik}-\omega)^2+\Gamma^2} \quad \text{with} \quad \Gamma = \gamma/2\,. \tag{3.10b}$$

With $x = (\omega_{ik}-\omega)/\Gamma$ this can be abbreviated as

$$g(\omega-\omega_{ik}) = \frac{1}{1+x^2} \quad \text{with} \quad g(\omega_{ik}) = 1\,. \tag{3.10c}$$

In this notation the area under the line profile becomes

$$\int_0^\infty I(\omega)\,\mathrm{d}\omega = \Gamma\int_{-\infty}^{+\infty} I(x)\,\mathrm{d}x = \pi I_0\Gamma\,. \tag{3.10d}$$

### 3.1.2 Relation Between Linewidth and Lifetime

The radiant power of the damped oscillator can be obtained from (3.3) if both sides of the equation are multiplied by $m\dot{x}$, which yields after rearranging

$$m\ddot{x}\dot{x} + m\omega_0^2 x\dot{x} = -\gamma m\dot{x}^2\,. \tag{3.12}$$

The left-hand side of (3.12) is the time derivative of the total energy $W$ (sum of kinetic energy $\frac{1}{2}m\dot{x}^2$ and potential energy $Dx^2/2 = m\omega_0^2 x^2/2$), and can therefore be written as

$$\frac{\mathrm{d}}{\mathrm{d}t}\left(\frac{m}{2}\dot{x}^2 + \frac{m}{2}\omega_0^2 x^2\right) = \frac{\mathrm{d}W}{\mathrm{d}t} = -\gamma m\dot{x}^2 \,. \tag{3.13}$$

Inserting $x(t)$ from (3.5) and neglecting terms with $\gamma^2$ yields

$$\frac{\mathrm{d}W}{\mathrm{d}t} = -\gamma m x_0^2 \omega_0^2 \,\mathrm{e}^{-\gamma t} \sin^2 \omega_0 t \,. \tag{3.14}$$

Because the time average $\overline{\sin^2 \omega t} = 1/2$, the time-averaged radiant power $\overline{P} = \overline{\mathrm{d}W/\mathrm{d}t}$ is

$$\overline{\frac{\mathrm{d}W}{\mathrm{d}t}} = -\frac{\gamma}{2} m x_0^2 \omega_0^2 \,\mathrm{e}^{-\gamma t} \,. \tag{3.15}$$

Equation (3.15) shows that $\overline{P}$ and with it the intensity $I(t)$ of the spectral line decreases to $1/\mathrm{e}$ of its initial value $I(t=0)$ after the decay time $\tau = 1/\gamma$.

In Sect. 2.8 we saw that the mean lifetime $\tau_i$ of a molecular level $E_i$, which decays exponentially by spontaneous emission, is related to the Einstein coefficient $A_i$ by $\tau_i = 1/A_i$. Replacing the classical damping constant $\gamma$ by the spontaneous transition probability $A_i$, we can use the classical formulas (3.9–3.11) as a correct description of the frequency distribution of spontaneous emission and its linewidth. The natural halfwidth of a spectral line spontaneously emitted from the level $E_i$ is, according to (3.11),

$$\delta\nu_n = A_i/2\pi = (2\pi\tau_i)^{-1} \quad \text{or} \quad \delta\omega_n = A_i = 1/\tau_i \,. \tag{3.16}$$

The radiant power emitted from $N_i$ excited atoms on a transition $E_i \to E_k$ is given by

$$\mathrm{d}W_{ik}/\mathrm{d}t = N_i A_{ik} \hbar\omega_{ik} \,. \tag{3.17}$$

If the emission of a source with volume $\Delta V$ is isotropic, the radiation power received by a detector of area $A$ at a distance $r$ through the solid angle $\mathrm{d}\Omega = A/r^2$ is

$$P_{ik} = \left(\frac{\mathrm{d}W_{ik}}{\mathrm{d}t}\right)\frac{\mathrm{d}\Omega}{4\pi} = N_i A_{ik} \hbar\omega_{ik} \Delta V \frac{A}{4\pi r^2} \,. \tag{3.18}$$

This means that the density $N_i$ of emitters can be inferred from the measured power, if $A_{ik}$ is known (Vol. 2, Sect. 6.3).

**Note:** Equation (3.16) can also be derived from the uncertainty principle (Fig. 3.3). With the mean lifetime $\tau_i$ of the excited level $E_i$, its energy $E_i$ can be determined only with an uncertainty $\Delta E_i \simeq \hbar/\tau_i$ [3.5]. The frequency $\omega_{ik} = (E_i - E_k)/\hbar$ of a transition terminating in the stable ground state $E_k$ has therefore the uncertainty

$$\delta\omega = \Delta E_i/\hbar = 1/\tau_i \,. \tag{3.19}$$

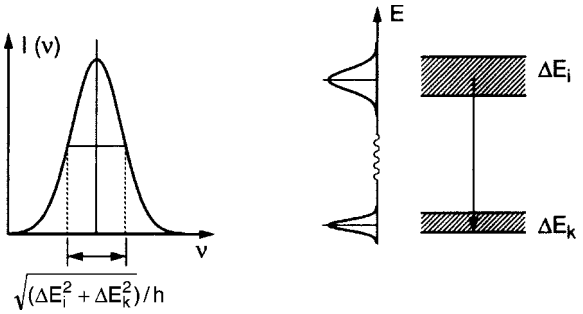


**Fig. 3.3.** Illustration of the uncertainty principle, which relates the natural linewidth to the energy uncertainties of the upper and lower levels

If the lower level $E_k$ is not the ground state but also an excited state with the lifetime $\tau_k$, the uncertainties $\Delta E_i$ and $\Delta E_k$ of the two levels both contribute to the linewidth. This yields for the total uncertainty

$$\Delta E = \sqrt{\Delta E_i^2 + \Delta E_k^2} \rightarrow \delta\omega_n = \sqrt{(1/\tau_i^2 + 1/\tau_k^2)}\,. \tag{3.20}$$

### 3.1.3 Natural Linewidth of Absorbing Transitions

In a similar way, the spectral profile of an *absorption line* can be derived for atoms *at rest*: the intensity $I$ of a plane wave passing in the $z$-direction through an absorbing sample decreases along the distance $\mathrm{d}z$ by

$$\mathrm{d}I = -\alpha I\,\mathrm{d}z\,. \tag{3.21}$$

The absorption coefficient $\alpha_{ik}$ [$\mathrm{cm}^{-1}$] for a transition $|i\rangle \rightarrow |k\rangle$ depends on the population densities $N_i$, $N_k$ of the lower and upper levels, and on the optical absorption cross section $\sigma_{ik}$ [$\mathrm{cm}^2$] of each absorbing atom, see (2.42):

$$\alpha_{ik}(\omega) = \sigma_{ik}(\omega)[N_i - (g_i/g_k)N_k]\,, \tag{3.22}$$

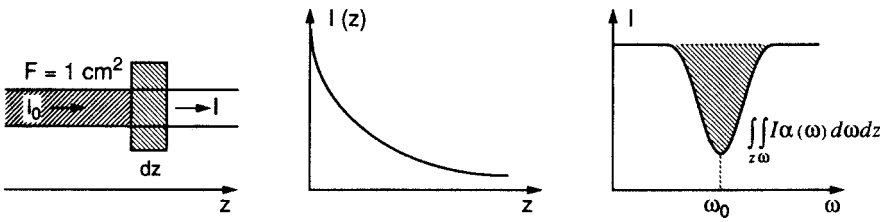


**Fig. 3.4.** Absorption of a parallel light beam passing through an optically thin absorbing layer

which reduces to $\alpha_{ik} = \sigma N_i$ for $N_k \ll N_i$ (Fig. 3.4). For sufficiently small intensities $I$, the induced absorption rate is small compared to the refilling rate of level $|i\rangle$ and the population density $N_i$ does not depend on the intensity $I$ (linear absorption). Integration of (3.21) then yields Beer's law

$$I = I_0 \, \mathrm{e}^{-\alpha(\omega) z} = I_0 \, \mathrm{e}^{-\sigma_{ik} N_i z} \, . \tag{3.23}$$

The absorption profile $\alpha(\omega)$ can be obtained from our classical model of a damped oscillator with charge $q$ under the influence of a driving force $qE$ caused by the incident wave with amplitude $E = E_0 \, \mathrm{e}^{\mathrm{i}\omega t}$. If the electric field amplitude is $\boldsymbol{E} = \{E_x, 0, 0\}$ the corresponding differential equation

$$m\ddot{x} + b\dot{x} + kx = qE_0 \, \mathrm{e}^{\mathrm{i}\omega t} \, , \tag{3.24}$$

has the solution

$$x = \frac{qE_0 \, \mathrm{e}^{\mathrm{i}\omega t}}{m(\omega_0^2 - \omega^2 + \mathrm{i}\gamma\omega)} \, , \tag{3.25}$$

with the abbreviations $\gamma = b/m$, and $\omega_0^2 = k/m$. The forced oscillation of the charge $q$ generates an induced dipole moment

$$p = qx = \frac{q^2 E_0 \, \mathrm{e}^{\mathrm{i}\omega t}}{m(\omega_0^2 - \omega^2 + \mathrm{i}\gamma\omega)} \, . \tag{3.26}$$

In a sample with $N$ oscillators per unit volume, the macroscopic polarization $P$, which is the sum of all dipole moments per unit volume, is therefore

$$P = Nqx \, . \tag{3.27}$$

On the other hand, the polarization can be derived in classical electrodynamics from Maxwell's equations using the dielectric constant $\epsilon_0$ or the susceptibility $\chi$, i.e.,

$$\boldsymbol{P} = \epsilon_0(\epsilon - 1)\boldsymbol{E} = \epsilon_0 \chi \boldsymbol{E} \, . \tag{3.28}$$

The relative dielectric constant $\epsilon$ is related to the refractive index $n$ by

$$n = \epsilon^{1/2} \, . \tag{3.29}$$

This can be easily verified from the relations

$$v = (\epsilon\epsilon_0\mu\mu_0)^{-1/2} = c/n \;\text{ and }\; c = (\epsilon_0\mu_0)^{-1/2} \quad \Rightarrow \quad n = \sqrt{\epsilon\mu} \, ,$$

for the velocity of light, which follows from Maxwell's equations in media with the dielectric constant $\epsilon_0\epsilon$ and the magnetic permeability $\mu_0\mu$. Except for ferromagnetic materials, the relative permeability is $\mu \simeq 1 \rightarrow n = \epsilon^{1/2}$.

Combining (3.25–3.29), the refractive index $n$ can be written as

$$n^2 = 1 + \frac{Nq^2}{\epsilon_0 m(\omega_0^2 - \omega^2 + \mathrm{i}\gamma\omega)} \, . \tag{3.30}$$

In gaseous media at sufficiently low pressures, the index of refraction is close to unity (for example, in air at atmospheric pressure, $n = 1.00028$ for $\lambda = 500\,\mathrm{nm}$). In this case, the approximation

$$n^2 - 1 = (n+1)(n-1) \simeq 2(n-1)\ ,$$

is sufficiently accurate for most purposes. Therefore (3.30) can be reduced to

$$n = 1 + \frac{Nq^2}{2\epsilon_0 m(\omega_0^2 - \omega^2 + \mathrm{i}\gamma\omega)}\ . \tag{3.31}$$

In order to make clear the physical implication of this complex index of refraction, we separate the real and the imaginary parts and write

$$n = n' - \mathrm{i}\kappa\ . \tag{3.32}$$

An EM wave $E = E_0 \exp[\mathrm{i}(\omega t - kz)]$ passing in the $z$-direction through a medium with the refractive index $n$ has the same frequency $\omega_n = \omega_0$ as in vacuum, but a different wave vector $k_n = k_0 n$. Inserting (3.32) with $|\boldsymbol{k}| = 2\pi/\lambda$ yields

$$E = E_0\,\mathrm{e}^{-k_0\kappa z}\,\mathrm{e}^{\mathrm{i}(\omega t - k_0 n' z)} = E_0\,\mathrm{e}^{-2\pi\kappa z/\lambda_0}\,\mathrm{e}^{\mathrm{i}k_0(ct - n' z)}\ . \tag{3.33}$$

Equation (3.33) shows that the imaginary part $\kappa(\omega)$ of the complex refractive index $n$ describes the *absorption* of the EM wave. At a penetration depth of $z = \lambda_0/(2\pi\kappa)$, the amplitude $E_0 \exp(-k_0\kappa z)$ has decreased to $1/\mathrm{e}$ of its value at $z = 0$. The real part $n'(\omega)$ represents the *dispersion* of the wave, i.e., the dependence of the phase velocity $v(\omega) = c/n'(\omega)$ on the frequency. The intensity $I \propto EE^*$ then decreases as

$$I = I_0\,\mathrm{e}^{-2\kappa k_0 z}\ . \tag{3.34}$$

Comparison with (3.23) yields the relation

$$\alpha = 2\kappa k_0 = 4\pi\kappa/\lambda_0\ . \tag{3.35}$$

*The absorption coefficient $\alpha$ is proportional to the imaginary part $\kappa$ of the complex refractive index $n = n' - \mathrm{i}\kappa$.*

The frequency dependence of $\alpha$ and $n'$ can be obtained by inserting (3.32, 3.35) into (3.31). Separating the real and imaginary parts, we get

$$\boxed{\alpha = \frac{Nq^2\omega_0}{c\epsilon_0 m}\,\frac{\gamma\omega}{(\omega_0^2 - \omega^2)^2 + \gamma^2\omega^2}\ ,} \tag{3.36a}$$

$$\boxed{n' = 1 + \frac{Nq^2}{2\epsilon_0 m}\,\frac{\omega_0^2 - \omega^2}{(\omega_0^2 - \omega^2)^2 + \gamma^2\omega^2}\ .} \tag{3.37a}$$

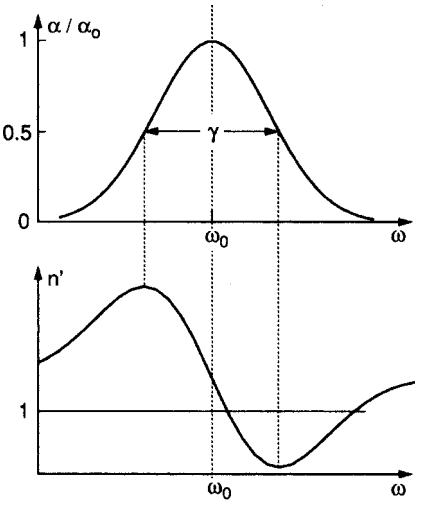


**Fig. 3.5.** Absorption coefficient $\alpha = 2k\kappa(\omega)$ and dispersion $n'(\omega)$ in the vicinity of an atomic transition with center frequency $\omega_0$

The equations (3.36a) and (3.37) are the *Kramers–Kronig dispersion relations*. They relate absorption and dispersion through the complex refractive index $n = n' - \mathrm{i}\kappa = n' - \mathrm{i}\alpha/(2k_0)$.

In the neighborhood of a molecular transition frequency $\omega_0$ where $|\omega_0 - \omega| \ll \omega_0$, the dispersion relations reduce with $q = \mathrm{e}$ and $\omega_0^2 - \omega^2 = (\omega_0 + \omega)(\omega_0 - \omega) \approx 2\omega_0(\omega_0 - \omega)$ to

$$\alpha(\omega) = \frac{N\mathrm{e}^2}{4\epsilon_0 m c} \frac{\gamma}{(\omega_0 - \omega)^2 + (\gamma/2)^2} , \tag{3.36b}$$

$$n' = 1 + \frac{N\mathrm{e}^2}{4\epsilon_0 m\omega_0} \frac{\omega_0 - \omega}{(\omega_0 - \omega)^2 + (\gamma/2)^2} . \tag{3.37b}$$

The absorption profile $\alpha(\omega)$ is Lorentzian with a FWHM of $\Delta\omega_n = \gamma$, which equals the natural linewidth. The difference $n' - n_0 = n' - 1$ between the refractive indices in a gas and in vacuum yields a dispersion profile.

Figure 3.5 shows the frequency dependence of $\alpha(\omega)$ and $n'(\omega)$ in the vicinity of the eigenfrequency $\omega_0$ of an atomic transition.

**Note:** The relations derived in this section are only valid for oscillators at rest in the observer's coordinate system. The thermal motion of real atoms in a gas introduces an additional broadening of the line profile, the *Doppler broadening*, which will be discussed in Sect. 3.2. The profiles (3.36, 3.37) can therefore be observed only with Doppler-free techniques (Vol. 2, Chaps. 2 and 4).

**Example 3.1.**

(a) The natural linewidth of the sodium $D_1$ line at $\lambda = 589.1\,\mathrm{nm}$, which corresponds to a transition between the $3P_{3/2}$ level ($\tau = 16\,\mathrm{ns}$) and the

$3S_{1/2}$ ground state, is

$$\delta\nu_n = \frac{10^9}{16 \times 2\pi} = 10^7\,\mathrm{s}^{-1} = 10\,\mathrm{MHz}\,.$$

Note that with a central frequency $\nu_0 = 5 \times 10^{14}\,\mathrm{Hz}$ and a lifetime of 16 ns, the damping of the corresponding classical oscillator is extremely small. Only after $8 \times 10^6$ periods of oscillation has the amplitude decreased to $1/\mathrm{e}$ of its initial value.

(b) The natural linewidth of a molecular transition between two vibrational levels of the electronic ground state with a wavelength in the infrared region is very small because of the long spontaneous lifetimes of vibrational levels. For a typical lifetime of $\tau = 10^{-3}\,\mathrm{s}$, the natural linewidth becomes $\delta\nu_n = 160\,\mathrm{Hz}$.

(c) Even in the visible or ultraviolet range, atomic or molecular electronic transitions with very small transition probabilities exist. In a dipole approximation these are "forbidden" transitions. One example is the $2\mathrm{s} \leftrightarrow 1\mathrm{s}$ transition for the hydrogen atom. The upper level 2s cannot decay by electric dipole transition, but a two-photon transition to the 1s ground state is possible. The natural lifetime is $\tau = 0.12\,\mathrm{s}$ and the natural linewidth of such a two-photon line is therefore $\delta\nu_n = 1.3\,\mathrm{Hz}$.

## 3.2 Doppler Width

Generally, the Lorentzian line profile with the natural linewidth $\delta\nu_n$, as discussed in Sect. 3.1, cannot be observed without special techniques, because it is completely concealed by other broadening effects. One of the major contributions to the spectral linewidth in gases at low pressures is the Doppler width, which is due to the thermal motion of the absorbing or emitting molecules.

Consider an excited molecule with a velocity $\boldsymbol{v} = \{v_x, v_y, v_z\}$ relative to the rest frame of the observer. The central frequency of a molecular emission line that is $\omega_0$ in the coordinate system of the molecule is Doppler shifted to

$$\omega_\mathrm{e} = \omega_0 + \boldsymbol{k} \cdot \boldsymbol{v}\,, \tag{3.38}$$

for an observer looking toward the emitting molecule (that is, against the direction of the wave vector $\boldsymbol{k}$ of the emitted radiation; Fig. 3.6a). For the observer, the apparent emission frequency $\omega_\mathrm{e}$ is increased if the molecule moves toward the observer ($\boldsymbol{k} \cdot \boldsymbol{v} > 0$), and decreased if the molecule moves away ($\boldsymbol{k} \cdot \boldsymbol{v} < 0$).

Similarly, one can see that the absorption frequency $\omega_0$ of a molecule moving with the velocity $\boldsymbol{v}$ across a plane EM wave $\boldsymbol{E} = \boldsymbol{E}_0 \exp(\mathrm{i}\omega t - \boldsymbol{k} \cdot \boldsymbol{r})$ is shifted. The wave frequency $\omega$ in the rest frame appears in the frame of the

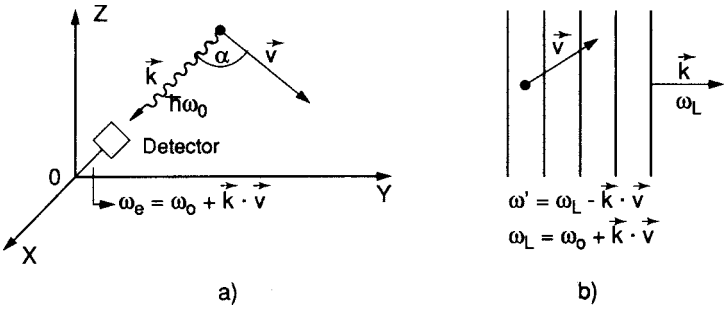


**Fig. 3.6.** (**a**) Doppler shift of a monochromatic emission line and (**b**) absorption line

moving molecule as

$$\omega' = \omega - \boldsymbol{k} \cdot \boldsymbol{v} \, .$$

The molecule can only absorb if $\omega'$ coincides with its eigenfrequency $\omega_0$. The absorption frequency $\omega = \omega_\mathrm{a}$ is then

$$\omega_\mathrm{a} = \omega_0 + \boldsymbol{k} \cdot \boldsymbol{v} \, . \tag{3.39a}$$

As in the emission case, the absorption frequency $\omega_\mathrm{a}$ is increased for $\boldsymbol{k} \cdot \boldsymbol{v} > 0$ (Fig. 3.6b). This happens, for example, if the molecule moves parallel to the wave propagation. It is decreased if $\boldsymbol{k} \cdot \boldsymbol{v} < 0$, e.g., when the molecule moves against the light propagation. If we choose the $+z$-direction to coincide with the light propagation, with $\boldsymbol{k} = \{0, 0, k_z\}$ and $|k| = 2\pi/\lambda$, (3.39a) becomes

$$\omega_\mathrm{a} = \omega_0 (1 + v_z/c) \, . \tag{3.39b}$$

**Note:** Equations (3.38) and (3.39) describe the *linear* Doppler shift. For higher accuracies, the quadratic Doppler effect must also be considered (Vol. 2, Sect. 9.1).

At thermal equilibrium, the molecules of a gas follow a Maxwellian velocity distribution. At the temperature $T$, the number of molecules $n_i(v_z)\,\mathrm{d}v_z$ in the level $E_i$ per unit volume with a velocity component between $v_z$ and $v_z + \mathrm{d}v_z$ is

$$n_i(v_z)\,\mathrm{d}v_z = \frac{N_i}{v_\mathrm{p}\sqrt{\pi}} \, \mathrm{e}^{-(v_z/v_\mathrm{p})^2} \, \mathrm{d}v_z \, , \tag{3.40}$$

where $N_i = \int n_i(v_z)\,\mathrm{d}v_z$ is the density of all molecules in level $E_i$, $v_\mathrm{p} = (2kT/m)^{1/2}$ is the most probable velocity, $m$ is the mass of a molecule, and $k$ is Boltzmann's constant. Inserting the relation (3.39b) between the velocity component and the frequency shift with $\mathrm{d}v_z = (c/\omega_0)\,\mathrm{d}\omega$ into (3.40) gives the number of molecules with absorption frequencies shifted from $\omega_0$ into the

interval from $\omega$ to $\omega + \mathrm{d}\omega$

$$n_i(\omega)\,\mathrm{d}\omega = N_i \frac{c}{\omega_0 v_\mathrm{p}\sqrt{\pi}} \exp\left[-\left(\frac{c(\omega-\omega_0)}{\omega_0 v_\mathrm{p}}\right)^2\right] \mathrm{d}\omega\,. \tag{3.41}$$

Since the emitted or absorbed radiant power $P(\omega)\,\mathrm{d}\omega$ is proportional to the density $n_i(\omega)\,\mathrm{d}\omega$ of molecules emitting or absorbing in the interval $\mathrm{d}\omega$, the intensity profile of a Doppler-broadened spectral line becomes

$$I(\omega) = I_0 \exp\left[-\left(\frac{c(\omega-\omega_0)}{\omega_0 v_\mathrm{p}}\right)^2\right]\,. \tag{3.42}$$

This is a Gaussian profile with a full halfwidth

$$\delta\omega_\mathrm{D} = 2\sqrt{\ln 2}\,\omega_0 v_\mathrm{p}/c = \left(\frac{\omega_0}{c}\right)\sqrt{8kT\ln 2/m}\,, \tag{3.43a}$$

which is called the *Doppler width*. Inserting (3.43) into (3.42) with $1/(4\ln 2) = 0.36$ yields

$$\boxed{I(\omega) = I_0 \exp\left(-\frac{(\omega-\omega_0)^2}{0.36\delta\omega_\mathrm{D}^2}\right)\,.} \tag{3.44}$$

Note that $\delta\omega_\mathrm{D}$ increases linearly with the frequency $\omega_0$ and is proportional to $(T/m)^{1/2}$. The largest Doppler width is thus expected for hydrogen ($M = 1$) at high temperatures and a large frequency $\omega$ for the Lyman $\alpha$ line.

Equation (3.43) can be written more conveniently in terms of the Avogadro number $N_\mathrm{A}$ (the number of molecules per mole), the mass of a mole, $M = N_\mathrm{A}m$, and the gas constant $R = N_\mathrm{A}k$. Inserting these relations into (3.43) for the Doppler width gives

$$\delta\omega_\mathrm{D} = (2\omega_0/c)\sqrt{2RT\ln 2/M}\,. \tag{3.43b}$$

or, in frequency units, using the values for $c$ and $R$,

$$\delta\nu_\mathrm{D} = 7.16\times10^{-7}\nu_0\sqrt{T/M} \quad [\mathrm{Hz}]\,. \tag{3.43c}$$

**Example 3.2.**

(a) Vacuum ultraviolet: for the Lyman $\alpha$ line ($2\mathrm{p} \rightarrow 1\mathrm{s}$ transition in the H atom) in a discharge with temperature $T = 1000\,\mathrm{K}$, $M = 1$, $\lambda = 121.6\,\mathrm{nm}$, $\nu_0 = 2.47\times10^{15}\,\mathrm{s}^{-1} \rightarrow \delta\nu_\mathrm{D} = 5.6\times10^{10}\,\mathrm{Hz}$, $\delta\lambda_\mathrm{D} = 2.8\times10^{-3}\,\mathrm{nm}$.

(b) Visible spectral region: for the sodium D line ($3\mathrm{p} \rightarrow 3\mathrm{s}$ transition of the Na atom) in a sodium-vapor cell at $T = 500\,\mathrm{K}$, $\lambda = 589.1\,\mathrm{nm}$, $\nu_0 = 5.1\times10^{14}\,\mathrm{s}^{-1} \rightarrow \delta\nu_\mathrm{D} = 1.7\times10^{9}\,\mathrm{Hz}$, $\delta\lambda_\mathrm{D} = 1\times10^{-3}\,\mathrm{nm}$.

(c) Infrared region: for a vibrational transition $(J_i, v_i) \leftrightarrow (J_k, v_k)$ between two rovibronic levels with the quantum numbers $J, v$ of the $CO_2$ molecule in a $CO_2$ cell at room temperature ($T = 300\,\mathrm{K}$), $\lambda = 10\,\mu\mathrm{m}$, $\nu = 3 \times 10^{13}\,\mathrm{s}^{-1}$, $M = 44 \rightarrow \delta\nu_\mathrm{D} = 5.6 \times 10^7\,\mathrm{Hz}$, $\delta\lambda_\mathrm{D} = 1.9 \times 10^{-2}\,\mathrm{nm}$.

These examples illustrate that in the visible and UV regions, the Doppler width exceeds the natural linewidth by about two orders of magnitude. Note, however, that the intensity $I$ approaches zero for large arguments $(\nu - \nu_0)$ much faster for a Gaussian line profile than for a Lorentzian profile (Fig. 3.7). It is therefore possible to obtain information about the Lorentzian profile from the extreme line wings, even if the Doppler width is much larger than the natural linewidth (see below).

More detailed consideration shows that a Doppler-broadened spectral line cannot be strictly represented by a pure Gaussian profile as has been assumed in the foregoing discussion, since not all molecules with a definite velocity component $v_z$ emit or absorb radiation at the same frequency $\omega' = \omega_0(1 + v_z/c)$. Because of the finite lifetimes of the molecular energy levels, the frequency response of these molecules is represented by a Lorentzian profile, see (3.10)

$$L(\omega - \omega') = \frac{\gamma/2\pi}{(\omega - \omega')^2 + (\gamma/2)^2} ,$$

with a central frequency $\omega'$ (Fig. 3.8). Let $n(\omega')\,\mathrm{d}\omega' = n(v_z)\,\mathrm{d}v_z$ be the number of molecules per unit volume with velocity components within the interval $v_z$ to $v_z + \mathrm{d}v_z$. The spectral intensity distribution $I(\omega)$ of the total absorption or emission of all molecules at the transition $E_i \rightarrow E_k$ is then

$$I(\omega) = I_0 \int n(\omega') L(\omega - \omega')\,\mathrm{d}\omega' . \tag{3.45}$$

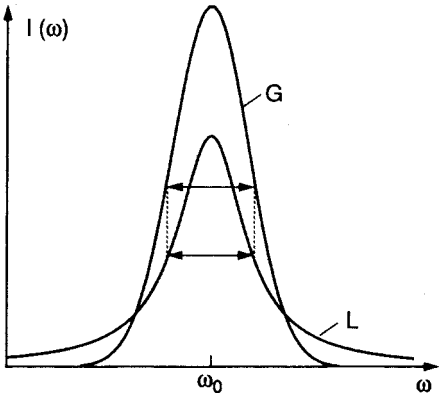


**Fig. 3.7.** Comparison between Lorentzian (L) and Gaussian (G) line profiles of equal halfwidths

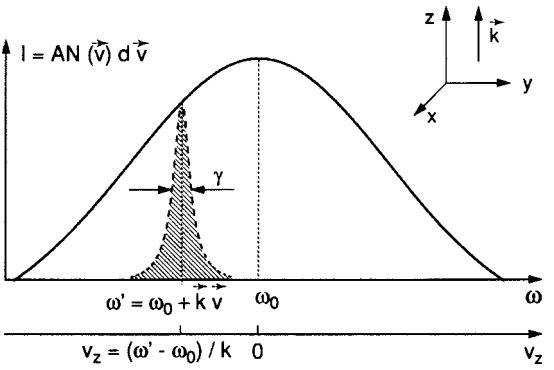


**Fig. 3.8.** Lorentzian profile centered at $\omega' = \omega_0 + \boldsymbol{k}\cdot\boldsymbol{v} = \omega_0(1 + v_z/c)$ for molecules with a definite velocity component $v_z$

Inserting (3.10) for $L(\omega-\omega')\,\mathrm{d}\omega'$ and (3.41) for $n(\omega')$, we obtain

$$I(\omega) = C\int_0^\infty \frac{\exp\{-[(c/v_\mathrm{p})(\omega_0-\omega')/\omega_0]^2\}}{(\omega-\omega')^2+(\gamma/2)^2}\,\mathrm{d}\omega' \tag{3.46}$$

with

$$C = \frac{\gamma N_i c}{2v_\mathrm{p}\pi^{3/2}\omega_0}\,.$$

This intensity profile, which is a convolution of Lorentzian and Gaussian profiles (Fig. 3.9), is called a *Voigt profile*. Voigt profiles play an important role in the spectroscopy of stellar atmospheres, where accurate measurements of line wings allow the contributions of Doppler broadening and natural linewidth or collisional line broadening to be separated (see [3.6] and Sect. 3.3). From such measurements the temperature and pressure of the emitting or absorbing layers in the stellar atmospheres may be deduced [3.7].

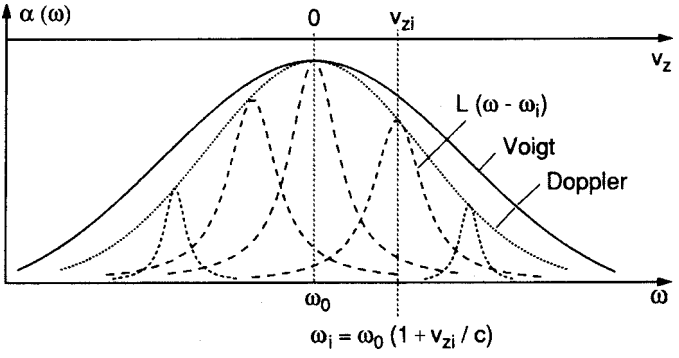


**Fig. 3.9.** Voigt profile as a convolution of Lorentzian line shapes $L(\omega_0-\omega_i)$ of molecules with different velocity components $v_{zi}$ and central absorption frequencies $\omega_i = \omega_0(1 + v_{zi}/c)$

## 3.3 Collisional Broadening of Spectral Lines

When an atom A with the energy levels $E_i$ and $E_k$ approaches another atom or molecule B, the energy levels of A are shifted because of the interaction between A and B. This shift depends on the electron configurations of A and B and on the distance $R(\mathrm{A}, \mathrm{B})$ between both collision partners, which we define as the distance between the centers of mass of A and B.

The energy shifts $\Delta E$ are, in general, different for the levels $E_i$ and $E_k$ and may be positive as well as negative. The energy shift $\Delta E$ is positive if the interaction between A and B is repulsive, and negative if it is attractive. When plotting the energy $E(R)$ for the different energy levels as a function of the interatomic distance $R$ typical potential curves of Fig. 3.10 are obtained.

This mutual interaction of both partners at distances $R \leq R_c$ is called a *collision* and radius $R_c$ is the *collision radius*. If no internal energy of the collision partners is transferred during the collision by nonradiative transitions, the collision is termed *elastic*. Without additional stabilizing mechanisms (recombination), the partners will separate again after the collision time $\tau_c \simeq R_c/v$, which depends on the relative velocity $v$.

**Example 3.3.**

At thermal velocities of $v = 5 \times 10^2$ m/s and a typical collision radius of $R_c = 1$ nm, we obtain the collision time $\tau_c = 2 \times 10^{-12}$ s. During this time the electronic charge distribution generally follows the perturbation "adiabatically", which justifies the potential curve model of Fig. 3.10.

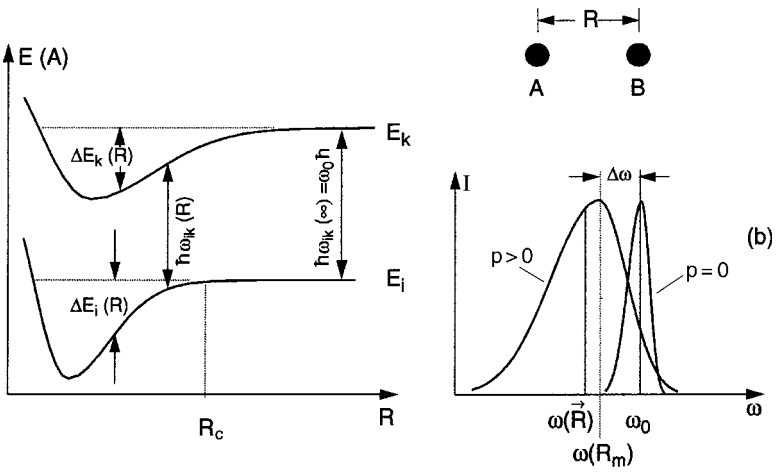


**Fig. 3.10.** Illustration of collisional line broadening explained with the potential curves of the collision pair AB

### 3.3.1 Phenomenological Description

If atom A undergoes a *radiative* transition between levels $E_i$ and $E_k$ during the collision time, the frequency

$$\omega_{ik} = |E_i(R) - E_k(R)| / \hbar \tag{3.47}$$

of absorbed or emitted radiation depends on the distance $R(t)$ at the time of the transition. We assume that the radiative transition takes place in a time interval that is short compared to the collision time, so that the distance $R$ does not change during the transition. In Fig. 3.10 this assumption leads to vertical radiative transitions.

In a gas mixture of atoms A and B, the mutual distance $R(\mathrm{A}, \mathrm{B})$ shows random fluctuations with a distribution around a mean value $\boldsymbol{R}$ that depends on pressure and temperature. According to (3.47), the fluorescence yields a corresponding frequency distribution around a most probable value $\omega_{ik}(R_\mathrm{m})$, which may be shifted against the frequency $\omega_0$ of the unperturbed atom A. The shift $\Delta\omega = \omega_0 - \omega_{ik}$ depends on how differently the two energy levels $E_i$ and $E_k$ are shifted at a distance $R_\mathrm{m}(\mathrm{A}, \mathrm{B})$ where the emission probability has a maximum. The intensity profile $I(\omega)$ of the collision-broadened and shifted emission line can be obtained from

$$I(\omega) \propto \int A_{ik}(R) P_\mathrm{col}(R) [E_i(R) - E_k(R)] \, \mathrm{d}R \,, \tag{3.48}$$

where $A_{ik}(R)$ is the spontaneous transition probability, which depends on $R$ because the electronic wave functions of the collision pair (AB) depend on $R$, and $P_\mathrm{col}(R)$ is the probability per unit time that the distance between A and B lies in the range from $R$ to $R + \mathrm{d}R$.

From (3.48) it can be seen that the intensity profile of the collision-broadened line reflects the difference of the potential curves

$$E_i(R) - E_k(R) = V[A(E_i), B] - V[A(E_k), B] \,.$$

Let $V(R)$ be the interaction potential between the ground-state atom A and its collision partner B. The probability that B has a distance between $R$ and $R + \mathrm{d}R$ is proportional to $4\pi R^2 \, \mathrm{d}R$ and (in thermal equilibrium) to the Boltzmann factor $\exp[-V(R)/kT]$. The number $N(R)$ of collision partners B with distance $R$ from A is therefore

$$N(R) \, \mathrm{d}R = N_0 4\pi R^2 \, \mathrm{e}^{-V(R)/kT} \, \mathrm{d}R \,, \tag{3.49}$$

where $N_0$ is the average density of atoms B. Because the intensity of an absorption line is proportional to the density of absorbing atoms while they are forming collision pairs, the intensity profile of the absorption line can be written as

$$I(\omega) \, \mathrm{d}\omega = C^* \left\{ R^2 \exp\left( -\frac{V_i(R)}{kT} \right) \frac{\mathrm{d}}{\mathrm{d}R} [V_i(R) - V_k(R)] \right\} \mathrm{d}R \,, \tag{3.50}$$

where $\hbar\omega(R) = [V_i(R) - V_k(R)] \rightarrow \hbar\,\mathrm{d}\omega/\mathrm{d}R = \mathrm{d}[V_i(R) - V_k(R)]/\mathrm{d}R$ has been used. Measuring the line profile as a function of temperature yields

$$\frac{\mathrm{d}I(\omega, T)}{\mathrm{d}T} = \frac{V_i(R)}{kT^2} I(\omega, T) ,$$

and therefore the ground-state potential $V_i(R)$ separately.

Frequently, different *spherical model potentials* $V(R)$ are substituted in (3.50), such as the Lennard–Jones potential

$$V(R) = a/R^{12} - b/R^6 , \tag{3.51}$$

The coefficients $a, b$ are adjusted for optimum agreement between theory and experiment [3.8–3.16].

The line shift caused by elastic collisions corresponds to an energy shift $\Delta E = \hbar\Delta\omega$ between the excitation energy $\hbar\omega_0$ of the free atom A* and the photon energy $\hbar\omega$. It is supplied from the kinetic energy of the collision partners. This means that in case of positive shifts ($\Delta\omega > 0$), the kinetic energy is smaller after the collision than before.

Besides elastic collisions, inelastic collisions may also occur in which the excitation energy $E_i$ of atom A is either partly or completely transferred into internal energy of the collision partner B, or into translational energy of both partners. Such inelastic collisions are often called *quenching collisions* because they decrease the number of excited atoms in level $E_i$ and therefore quench the fluorescence intensity. The total transition probabiltiy $A_i$ for the depopulation of level $E_i$ is a sum of radiative and collision-induced probabilities (Fig. 2.15)

$$A_i = A_i^{\mathrm{rad}} + A_i^{\mathrm{coll}} \quad \text{with} \quad A_i^{\mathrm{coll}} = N_B \sigma_i \boldsymbol{v} . \tag{3.52}$$

Inserting the relations

$$\boldsymbol{v} = \sqrt{\frac{8kT}{\pi\mu}} , \quad \mu = \frac{M_\mathrm{A} \cdot M_\mathrm{B}}{M_\mathrm{A} + M_\mathrm{B}} , \quad p_\mathrm{B} = N_\mathrm{B} kT ,$$

between the mean relative velocity $\boldsymbol{v}$, the responsible pressure $p_\mathrm{B}$, and the gas temperature $T$ into (3.52) gives the total transition probability

$$A_i = \frac{1}{\tau_\mathrm{sp}} + a p_\mathrm{B} \quad \text{with} \quad a = 2\sigma_{ik}\sqrt{\frac{2}{\pi\mu kT}} . \tag{3.53}$$

It is evident from (3.16) that this pressure-dependent transition probability causes a corresponding pressure-dependent linewidth $\delta\omega$, which can be described by a sum of two damping terms

$$\delta\omega = \delta\omega_n + \delta\omega_\mathrm{col} = \gamma_n + \gamma_\mathrm{col} = \gamma_n + a p_\mathrm{B} . \tag{3.54}$$

The collision-induced additional line broadening $a p_\mathrm{B}$ is therefore often called *pressure broadening*.

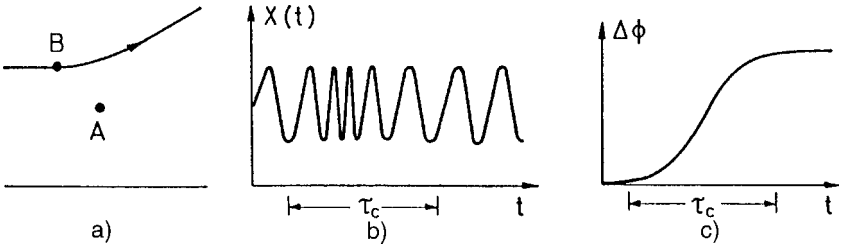


**Fig. 3.11a–c.** Phase perturbation of an oscillator by collisions: (**a**) classical path approximation of colliding particles; (**b**) frequency change of the oscillator $A(t)$ during the collision; (**c**) resulting phase shift

From the derivation in Sect. 3.1, one obtains a Lorentzian profile (3.9) with a halfwidth $\gamma = \gamma_n + \gamma_{\text{col}}$ for the line broadened by inelastic collisions:

$$I(\omega) = \frac{C}{(\omega - \omega_0)^2 + [(\gamma_n + \gamma_{\text{col}})/2]^2} \,. \tag{3.55}$$

The *elastic collisions* do not change the amplitude, but the *phase* of the damped oscillator is changed due to the frequency shift $\Delta\omega(R)$ during the collisions. They are often termed *phase-perturbing collisions* (Fig. 3.11).

When taking into account line shifts $\Delta\omega$ caused by elastic collisions, the line profile for cases where it still can be described by a Lorentzian becomes

$$I(\omega) = \frac{C^*}{(\omega - \omega_0 - \Delta\omega)^2 + (\gamma/2)^2} \,, \tag{3.56}$$

where the line shift

$$\Delta\omega = N_{\text{B}} \cdot \overline{v} \cdot \sigma_{\text{s}}$$

and the line broadening

$$\gamma = \gamma_n + N_{\text{B}} \cdot \overline{v} \cdot \sigma_{\text{b}}$$

are determined by the number density $N_{\text{B}}$ of collision parameters B and by the collision cross sections $\sigma_{\text{s}}$ for line shifts and $\sigma_{\text{b}}$ for broadening (Fig. 3.12).

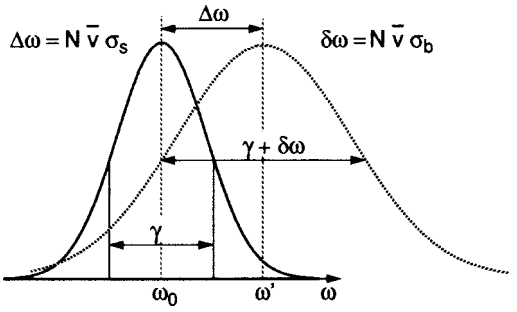


**Fig. 3.12.** Shift and broadening of a Lorentzian line profile by collisions

**Table 3.1.** Broadening (fullhalfwidth $\gamma/n$) and shift $\Delta\omega/n$ of atomic alkali resonance lines by noble gases and $N_2$. (All numbers are given in units of $10^{-20}\,\mathrm{cm}^{-1}/\mathrm{cm}^{-3} \approx 10\,\mathrm{MHz/torr}$ at $T = 300\,\mathrm{K}$)

| | Transition | λ (nm) | Self-broadening | Helium width | Helium Shift | Neon width | Neon Shift | Argon width | Argon Shift | Krypton width | Krypton Shift | Xenon width | Xenon Shift | Nitrogen width | Nitrogen Shift |
|---|---|---|---|---|---|---|---|---|---|---|---|---|---|---|---|
| Li | $2S$–$2P$ | 670.8 | $2.5\times10^2$ | 2.2 | −0.08 | 1.5 | −0.2 | 2.4 | −0.7 | 2.9 | −0.8 | 3.3 | −1.0 | | |
| Na | $3S_{1/2}$–$3P_{1/2}$ | 598.6 | $1.6\times10^2$ | 1.6 | 0.00 | 1.3 | −0.3 | 2.9 | −0.85 | 2.8 | −0.6 | 3.0 | −0.6 | 1.8 | −0.8 |
| | $-P_{3/2}$ | 598.0 | $2.7\times10^2$ | 3.0 | −0.06 | 1.5 | −0.75 | 2.3 | −0.7 | 2.5 | −0.7 | 2.5 | −0.7 | | |
| K | $4S_{1/2}$–$4P_{1/2}$ | 769.9 | $3.2\times10^2$ | 1.5 | +0.24 | 0.9 | −0.22 | 2.6 | −1.2 | 2.4 | −0.9 | 2.9 | −1.0 | 2.6 | −1.0 |
| | $-4P_{3/2}$ | 766.5 | $2.2\times10^2$ | 2.1 | +0.13 | 1.2 | −0.33 | 2.1 | −0.8 | 2.5 | −0.6 | 2.9 | −1.0 | 2.6 | −0.7 |
| | $-5P_{1/2}$ | 404.7 | $0.8\times10^1$ | 3.8 | +0.74 | 1.6 | 0.0 | 7.2 | −2.0 | 6.6 | −2.0 | 6.6 | | | |
| Rb | $5S_{1/2}$–$5P_{1/2}$ | 794.7 | $3.7\times10^2$ | 2.0 | 1.0 | 1.0 | −0.04 | 2.0 | −0.8 | 2.3 | −0.8 | | | | |
| | $-6P_{1/2}$ | 421.6 | $1.6\times10^1$ | | | | | | | | | | | | |
| | $-10P_{1/2}$ | 315.5 | $0.4\times10^1$ | 5.0 | | | | | −9.5 | | | | −6 | | |
| Cs | $6S_{1/2}$–$6P_{1/2}$ | 894.3 | | 2.0 | +0.67 | 1.0 | −0.29 | 2.0 | −0.9 | 2.0 | −0.27 | 2.1 | −0.8 | 3.1 | −0.7 |
| | $-7P_{1/2}$ | 459.0 | | 8.8 | +1.0 | 3.5 | 0.0 | 8.6 | −1.6 | | −1.5 | 6.3 | −1.7 | | |

**Note**: The values differ quite substantially in the literature. Therefore some average values were used in Table 3.1.

References: N. Allard, J. Kielkopf: Rev. Med. Phys. **54**, 1103 (1982)
M.J. O'Callaghan, A. Gallagher: Phys. Rev. **39**, 6190 (1989)
E. Schüler, W. Behmenburg: Phys. Rep. **12C**, 274 (1974)

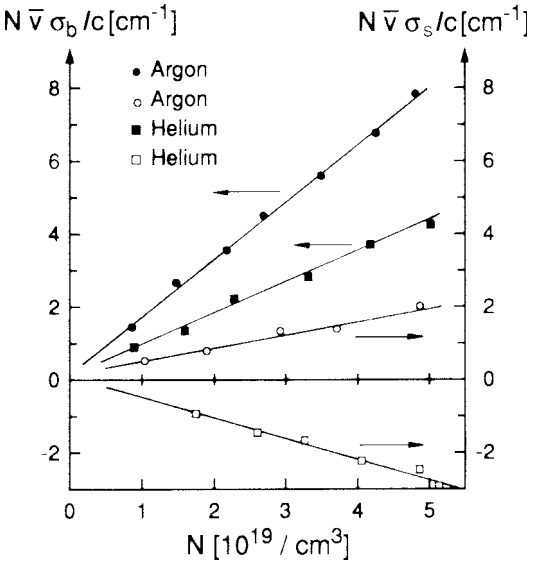


**Fig. 3.13.** Pressure broadening (*left scale*) and shifts (*right scale*) of the lithium resonance line by different noble gases [3.17]

The constant $C^* = (I_0/2\pi)(\gamma + N_B \overline{v}\sigma_b)$ becomes $I_0\gamma/2\pi$ for $N_B = 0$, when (3.56) becomes identical to (3.10).

**Note:** The real collision-induced line profile depends on the interaction potential between A and B. In most cases it is no longer Lorentzian, but has an asymmetric profile because the transition probability depends on the internuclear distance and because the energy difference $\Delta E(R) = E_i(R) - E_k(R)$ is generally not a uniformly rising or falling function but may have extrema.

Figure 3.13 depicts as examples pressure broadening and shifts in [$cm^{-1}$] of the lithium resonance line perturbed by different noble gas atoms. Table 3.1 compiles pressure-broadening and line shift data for different alkali resonance lines.

### 3.3.2 Relations Between Interaction Potential, Line Broadening, and Shifts

In order to gain more insight into the physical meaning of the cross sections $\sigma_s$ and $\sigma_b$, we have to discover the relation between the phase shift $\eta(R)$ and the potential $V(R)$. Assume potentials of the form

$$V_i(R) = C_i/R^n\,, \quad V_k(R) = C_k/R^n\,, \tag{3.57}$$

between the atom in level $E_i$ or $E_k$ and the perturbing atom B. The frequency shift $\Delta\omega$ for the transition $E_i \rightarrow E_k$ is then

$$\hbar\Delta\omega(R) = \frac{C_i - C_k}{R^n}\,. \tag{3.58}$$

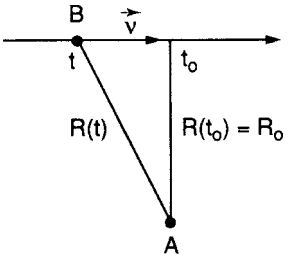


**Fig. 3.14.** Linear path approximation of a collision between A and B

The line broadening comes from two contributions:

(a) The phase shift, due to the frequency shift of the oscillator during the collision
(b) the quenching collisions which shorten the effective lifetime of the upper level of $A$.

The corresponding phase shift of the oscillator $A$ due to a collision with impact parameter $R_0$, where we neglect the scattering of B and assume that the path of B is not deflected but follows a straight line (Fig. 3.14), is

$$\Delta\phi(R_0) = \int_{-\infty}^{+\infty} \Delta\omega \, \mathrm{d}t = \frac{1}{\hbar} \int_{-\infty}^{+\infty} \frac{(C_i - C_k)\,\mathrm{d}t}{[R_0^2 + \overline{v}^2 (t - t_0)^2]^{n/2}} = \frac{\alpha_n (C_i - C_k)}{\boldsymbol{v} R_0^{n-1}} \,. \tag{3.59}$$

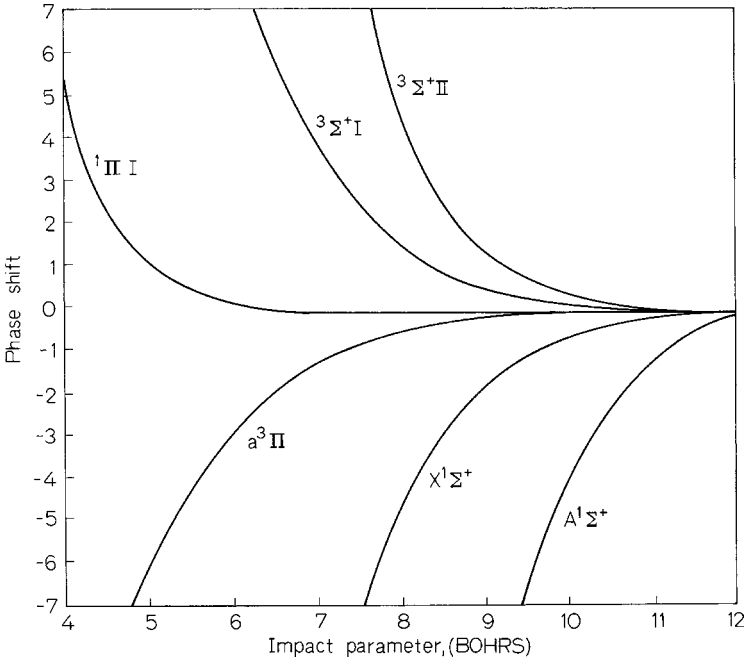


**Fig. 3.15.** Phase shift of the Na*(3p) oscillation for Na*–H collisions versus impact parameter. The various adiabatic molecular states for Na*H are indicated [3.12]

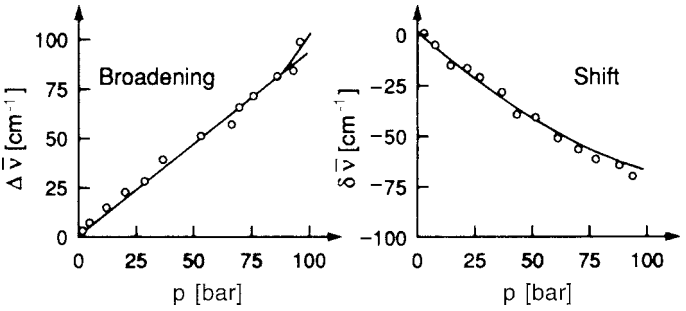


**Fig. 3.16.** Broadening and shift of the Cs resonance line at $\lambda = 894.3\,\text{nm}$ by argon

Equation (3.59) provides the relation between the phase shift $\Delta\phi(R_0)$ and the difference (3.58) of the interaction potentials, where $\alpha_n$ is a numerical constant depending on the exponent $n$ in (3.58).

The phase shifts may be positive ($C_i > C_k$) or negative depending on the relative orientation of spin and angular momenta. This is illustrated by Fig. 3.15, which shows the phase shifts of the Na atom, oscillating on the 3s–3p transition for Na–H collisions at large impact parameters [3.12].

It turns out that the main contribution to the line broadening cross section $\sigma_b$ comes from collisions with *small* impact parameters, whereas the lineshift cross section $\sigma_s$ still has large values for *large* impact parameters. This means that elastic *collisions at large distances do not cause noticeable broadening of the line, but can still very effectively shift the line center* [3.18]. Figure 3.16 exhibits broadening and shift of the Cs resonance line by argon atoms.

Nonmonotonic interaction potentials $V(R)$, such as the Lennard–Jones potential (3.51), cause satellites in the wings of the broadened profiles (Fig. 3.17) From the satellite structure the interaction potential may be deduced [3.19].

Because of the long-range Coulomb interactions between charged particles (electrons and ions) described by the potential (3.57) with $n = 1$, pressure broadening and shift is particularly large in plasmas and gas discharges [3.20, 3.21]. This is of interest for gas discharge lasers, such as the HeNe laser or the argon-ion laser [3.22, 3.23]. The interaction between charged particles can be described by the linear and quadratic Stark effects. It can be shown that the linear Stark effect causes only line broadening, while the quadratic effect also leads to line shifts. From measurements of line profiles in plasmas, very detailed plasma characteristics, such as electron or ion densities and temperatures, can be determined. Plasma spectroscopy has therefore become an extensive field of research [3.24], of interest not only for astrophysics, but also for fusion research in high-temperature plasmas [3.25]. Lasers play an important role in accurate measurements of line profiles in plasmas [3.26–3.29].

The classical models used to explain collisional broadening and line shifts can be improved by using quantum mechanical calculations. These are, however, beyond the scope of this book, and the reader is referred to the literature [3.1, 3.14, 3.22–3.34].

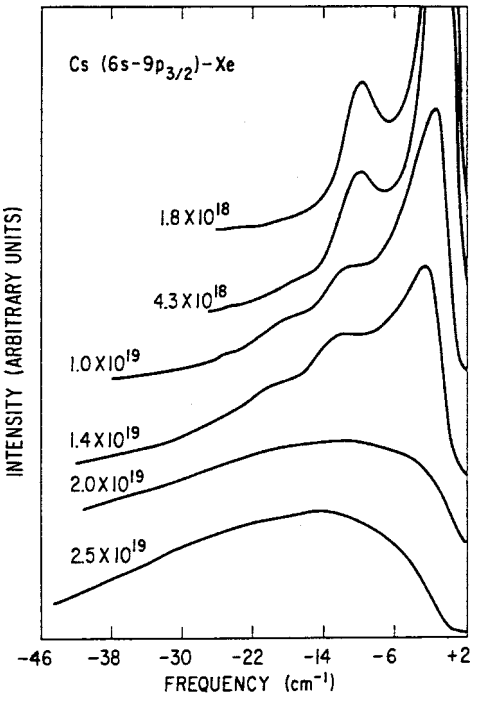


**Fig. 3.17.** Satellites in the pressure-broadened line profile of the cesium transition $6s \rightarrow 9p_{3/2}$ for Cs–Xe collisions at different xenon densities [atoms/cm$^3$] [3.14]

**Example 3.4.**

(a) The pressure broadening of the sodium D line $\lambda = 589\,\text{nm}$ by argon is $2.3 \times 10^{-5}\,\text{nm/mbar}$, equivalent to $0.228\,\text{MHz/Pa}$. The shift is about $-1\,\text{MHz/torr}$. The self-broadening of 150 MHz/torr due to collisions between Na atoms is much larger. However, at pressures of several torr, the pressure broadening is still smaller than the Doppler width.

(b) The pressure broadening of molecular vibration–rotation transitions with wavelengths $\lambda \simeq 5\,\mu\text{m}$ is a few MHz/torr. At atmospheric pressure, the collisional broadening therefore exceeds the Doppler width. For example, the rotational lines of the $\nu_2$ band of $H_2O$ in air at normal pressure (760 torr) have a Doppler width of 150 MHz, but a pressure-broadened linewidth of 930 MHz.

(c) The collisional broadening of the red neon line at $\lambda = 633\,\text{nm}$ in the low-pressure discharge of a HeNe laser is about $\delta\nu = 150\,\text{MHz/torr}$; the pressure shift $\Delta\nu = 20\,\text{MHz/torr}$. In high-current discharges, such as the argon laser discharge, the degree of ionization is much higher than in the HeNe laser and the Coulomb interaction between ions and electrons plays a major role. The pressure broadening is therefore much larger: $\delta\nu = 1500\,\text{MHz/torr}$. Because of the high temperature in the plasma, the Doppler width $\delta\nu_D \simeq 5000\,\text{MHz}$ is even larger [3.23].

### 3.3.3 Collisional Narrowing of Lines

In the infrared and microwave ranges, collisions may sometimes cause a narrowing of the linewidth instead of a broadening (*Dicke narrowing*) [3.35]. This can be explained as follows: if the lifetime of the upper molecular level (e.g., an excited vibrational level in the electronic ground state) is long compared to the mean time between successive collisions, the velocity of the oscillator is often altered by elastic collisions and the mean velocity component is smaller than without these collisions, resulting in a smaller Doppler shift. When the Doppler width is larger than the pressure-broadened width, this effect causes a narrowing of the Doppler-broadened lines, if the mean-free path is smaller than the wavelength of the molecular transition [3.36]. Figure 3.18 illustrates this Dicke narrowing for a rotational transition of the $H_2O$ molecule at $\lambda = 5.34\,\mu m$. The linewidth decreases with increasing pressure up to pressures of about 100−150 torr, depending on the collision partner, which determines the mean-free path $\Lambda$. For higher pressures, the pressure broadening overcompensates the Dicke narrowing, and the linewidth increases again.

There is a second effect that causes a collisional narrowing of spectral lines. In the case of very long lifetimes of levels connected by an EM transition, the linewidth is not determined by the lifetimes but by the diffusion time of the atoms out of the laser beam (Sect. 3.4). Inserting a noble gas into the sample cell decreases the diffusion rate and therefore increases the interaction time of the sample atoms with the laser field, which results in a decrease of the linewidth with pressure [3.37] until the pressure broadening overcompensates the narrowing effect.

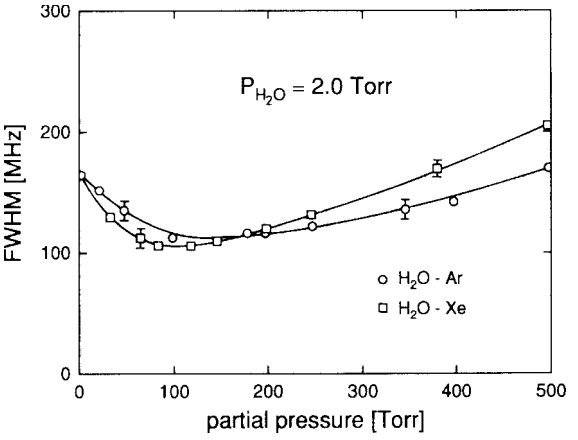


**Fig. 3.18.** Dicke narrowing and pressure broadening of a rotational transition in $H_2O$ at $1871\,cm^{-1}$ ($\lambda = 5.3\,\mu m$) as a function of Ar and Xe pressure [3.36]

## 3.4 Transit-Time Broadening

In many experiments in laser spectroscopy, the interaction time of molecules with the radiation field is small compared with the spontaneous lifetimes of excited levels. Particularly for transitions between rotational–vibrational levels of molecules with spontaneous lifetimes in the millisecond range, the transit time $T = d/|\boldsymbol{v}|$ of molecules with a mean thermal velocity $\boldsymbol{v}$ passing through a laser beam of diameter $d$ may be smaller than the spontaneous lifetime by several orders of magnitude.

**Example 3.5.**

(a) Molecules in a molecular beam with thermal velocities $|\boldsymbol{v}| = 5 \times 10^4$ cm/s passing through a laser beam of 0.1-cm diameter have the mean transit time $T = 2\,\mu$s.
(b) For a beam of fast ions with velocities $\overline{v} = 3 \times 10^8$ cm/s, the time required to traverse a laser beam with $d = 0.1$ cm is already below $10^{-9}$ s, which is shorter than the spontaneous lifetimes of most atomic levels.

In such cases, the linewidth of a Doppler-free molecular transition is no longer limited by the spontaneous transition probabilities (Sect. 3.1), but by the time of flight through the laser beam, which determines the interaction time of the molecule with the radiation field. This can be seen as follows: consider an undamped oscillator $x = x_0 \cos \omega_0 t$ that oscillates with constant amplitude during the time interval $T$ and then suddenly stops oscillating. Its frequency spectrum is obtained from the Fourier transform

$$A(\omega) = \frac{1}{\sqrt{2\pi}} \int_0^T x_0 \cos(\omega_0 t)\, \mathrm{e}^{-\mathrm{i}\omega t}\, \mathrm{d}t\,. \tag{3.60}$$

The spectral intensity profile $I(\omega) = A^* A$ is, for $(\omega - \omega_0) \ll \omega_0$,

$$I(\omega) = C \frac{\sin^2[(\omega - \omega_0)T/2]}{(\omega - \omega_0)^2}\,, \tag{3.61}$$

according to the discussion in Sect. 3.1. This is a function with a full halfwidth $\delta\omega_\mathrm{T} = 5.6/T$ of its central maximum (Fig. 3.19a) and a full width $\delta\omega_\mathrm{b} = 4\pi/T \simeq 12.6/T$ between the zero points on both sides of the central maximum.

This example can be applied to an atom that traverses a laser beam with a rectangular intensity profile (Fig. 3.19a). The oscillator amplitude $x(t)$ is proportional to the field amplitude $E = E_0(\boldsymbol{r}) \cos \omega t$. If the interaction time $T = d/v$ is small compared to the damping time $T = 1/\gamma$, the oscillation amplitude can be regarded as constant during the time $T$. The full halfwidth of the absorption line is then $\delta\omega = 5.6v/d \rightarrow \delta\nu \simeq v/d$.

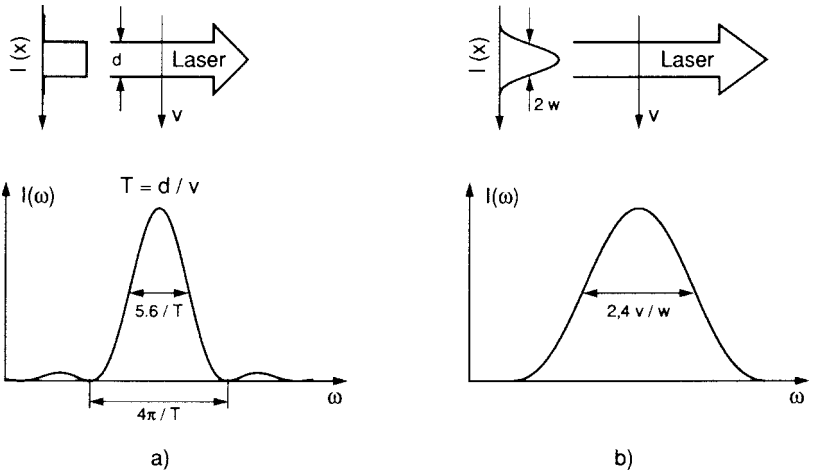


**Fig. 3.19a,b.** Transition probability $\mathcal{P}(\omega)$ of an atom traversing a laser beam (**a**) with a rectangular intensity profile $I(x)$; and (**b**) with a Gaussian intensity profile for the case $\gamma < 1/T = v/d$. The intensity profile $I(\omega)$ of an absorption line is proportional to $\mathcal{P}(\omega)$

In reality, the field distribution across a laser beam that oscillates in the fundamental mode is given by (Sect. 5.3)

$$E = E_0 \, \mathrm{e}^{-r^2/w^2} \cos \omega t \, ,$$

in which $2w$ gives the diameter of the Gaussian beam profile across the points where $E = E_0/\mathrm{e}$. Substituting the forced oscillator amplitude $x = \alpha E$ into (3.60), one obtains instead of (3.61) a Gaussian line profile (Fig. 3.19b)

$$I(\omega) = I_0 \exp\left(-(\omega - \omega_0)^2 \frac{w^2}{2v^2}\right) \, , \tag{3.62}$$

with a transit-time limited halfwidth (FWHM)

$$\delta\omega_{\mathrm{tt}} = 2(v/w)\sqrt{2\ln(2)} \simeq 2.4 v/w \rightarrow \delta\nu \simeq 0.4 v/w \, . \tag{3.63}$$

The quantity $w = (\lambda R/2\pi)^{1/2}$ (see Sect. 5.2.3) is called the beam waist of the Gaussian beam profile.

There are two possible ways of reducing the transit-time broadening: one may either enlarge the laser beam diameter $2w$, or one may decrease the molecular velocity $v$. Both methods have been verified experimentally and will be discussed in Vol. 2, Sects. 2.3 and 9.2. The most efficient way is to directly reduce the atomic velocity by optical cooling (Vol. 2, Chap. 9).

**Example 3.6.**

(a) A beam of $NO_2$ molecules with $\overline{v} = 600\,\mathrm{m/s}$ passes through a focused laser beam with $w = 0.1\,\mathrm{mm}$. Their transit time broadening $\delta\nu \simeq 1.2\,\mathrm{MHz}$ is large compared to their natural linewidth $\delta\nu_\mathrm{n} \simeq 10\,\mathrm{kHz}$ of optical transitions.

(b) For frequency standards the rotational–vibrational transition of $CH_4$ at $\lambda = 3.39\,\mu\mathrm{m}$ is used (Vol. 2, Sect. 2.3). In order to reduce the transit-time broadening for $CH_4$ molecules with $\overline{v} = 7 \times 10^4\,\mathrm{cm/s}$ below their natural linewidth of $\delta\nu = 10\,\mathrm{kHz}$, the laser-beam diameter must be enlarged to $2w \geq 6\,\mathrm{cm}$.

So far, we have assumed that the wave fronts of the laser radiation field are planes and that the molecules move parallel to these planes. However, the phase surfaces of a focused Gaussian beam are curved except at the focus. As Fig. 3.20 illustrates, an atom moving along the $r$-direction perpendicular to the laser beam $z$-axis experiences a maximum phase shift $\Delta\phi = x2\pi/\lambda$, between the points $r = 0$ and $r = r_1$. With $r^2 = R^2 - (R-x)^2$ we obtain the approximation $x \simeq r^2/2R$ for $x \ll R$. This gives for the phase shifts

$$\Delta\phi = kr^2/2R = \omega r^2/(2cR)\,, \tag{3.64}$$

where $k = \omega/c$ is the magnitude of the wave vector, and $R$ is the radius of curvature of the wave front. This phase shift depends on the location of an atom and is therefore different for the different atoms, and causes additional line broadening (Sect. 3.3.1). The calculation [3.38] yields for the transit-time broadened halfwidth, including the wave-front curvature,

$$\begin{aligned}\delta\omega &= \frac{2v}{w}\sqrt{2\ln 2}\left[1+\left(\frac{\pi w^2}{R\lambda}\right)^2\right]^{1/2} \\ &= \delta\omega_\mathrm{tt}\left[1+\left(\frac{\pi w^2}{R\lambda}\right)^2\right]^{1/2} \approx \delta\omega_\mathrm{tt}(1+\Delta\phi^2)^{1/2}\,.\end{aligned} \tag{3.65}$$

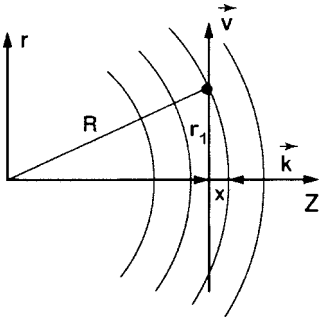


**Fig. 3.20.** Line broadening caused by the curvature of wave fronts

In order to minimize this additional broadening, the radius of curvature has to be made as large as possible. If $\Delta\phi \ll \pi$ for a distance $r = w$, the broadening by the wave-front curvature is small compared to the transit-time broadening. This imposes the condition $R \gg w^2/\lambda$ on the radius of curvature.

**Example 3.7.**

For a wave with $\lambda = 1\,\mu\text{m} \rightarrow \omega = 2\times10^{15}\,\text{Hz}$. With $w = 1\,\text{cm}$, this gives, according to (3.64), a maximum phase shift $\Delta\phi = 2\times10^{15}\,/\,(6\times10^{10}R$ [cm]). In order to keep $\Delta\phi \ll 2\pi$, the radius of curvature should be $R \gg 5\times10^3\,\text{cm}$. For $R = 5\times10^3\,\text{cm} \rightarrow \Delta\phi = 2\pi$ and the phase-front curvature causes an additional broadening by a factor of about 6.5.

## 3.5 Homogeneous and Inhomogeneous Line Broadening

If the probability $\mathcal{P}_{ik}(\omega)$ of absorption or emission of radiation with frequency $\omega$ causing a transition $E_i \rightarrow E_k$ is equal for all the molecules of a sample that are in the same level $E_i$, we call the spectral line profile of this transition *homogeneously broadened*. Natural line broadening is an example that yields a homogeneous line profile. In this case, the probability for emission of light with frequency $\omega$ on a transition $E_i \rightarrow E_k$ with the normalized Lorentzian profile $L(\omega-\omega_0)$ and central frequency $\omega_0$ is given by

$$\mathcal{P}_{ik}(\omega) = A_{ik}L(\omega-\omega_0)\ .$$

It is equal for all atoms in level $E_i$.

The standard example of inhomogeneous line broadening is Doppler broadening. In this case, the probability of absorption or emission of monochromatic radiation $E(\omega)$ is not equal for all molecules, but depends on their velocity $\overline{v}$ (Sect. 3.2). We divide the molecules in level $E_i$ into subgroups such that all molecules with a velocity component within the interval $v_z$ to $v_z + \Delta v_z$ belong to one subgroup. If we choose $\Delta v_z$ to be $\delta\omega_\text{n}/k$ where $\delta\omega_\text{n}$ is the natural linewidth, we may consider the frequency interval $\delta\omega_\text{n}$ to be homogeneously broadened inside the much larger inhomogeneous Doppler width. That is to say, all molecules in the subgroup can absorb or emit radiation with wave vector $\boldsymbol{k}$ and frequency $\omega = \omega_0 + v_z|\boldsymbol{k}|$ (Fig. 3.8), because in the coordinate system of the moving molecules, this frequency is within the natural width $\delta\omega_\text{n}$ around $\omega_0$ (Sect. 3.2).

In Sect. 3.3 we saw that the spectral line profile is altered by two kinds of collisions: Inelastic and elastic collisions. Inelastic collisions cause additional damping, resulting in pure broadening of the Lorentzian line profile. This broadening by inelastic collisions brings about a homogeneous Lorentzian line profile. The elastic collisions could be described as phase-perturbing collisions. The Fourier transform of the oscillation trains with random phase jumps again yields a Lorentzian line profile, as derived in Sect. 3.3. Summarizing,

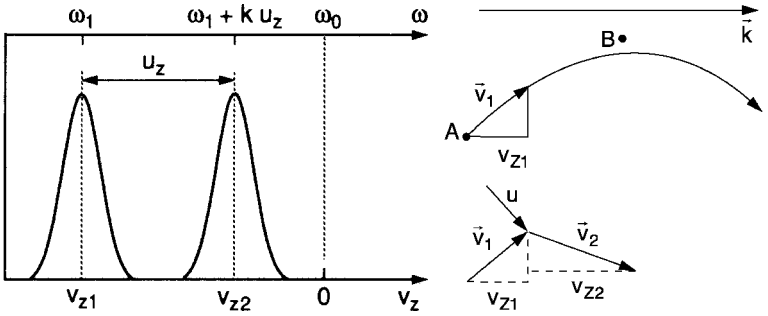


**Fig. 3.21.** Effect of velocity-changing collisions on the frequency shift of homogeneous subgroups within a Doppler-broadened line profile

we can state that elastic and inelastic collisions that only perturb the phase or amplitude of an oscillating atom without changing its velocity cause homogeneous line broadening.

So far, we have neglected the fact that collisions also change the velocity of both collision partners. If the velocity component $v_z$ of a molecule is altered by an amount $u_z$ during the collision, the molecule is transferred from one subgroup $(v_z \pm \Delta v_z)$ within the Doppler profile to another subgroup $(v_z + u_z \pm \Delta v_z)$. This causes a shift of its absorption or emission frequency from $\omega$ to $\omega + ku_z$ (Fig. 3.21). This shift should not be confused with the line shift caused by phase-perturbing elastic collisions that also occurs when the velocity of the oscillator does not noticeably change.

At thermal equilibrium, the changes $u_z$ of $v_z$ by velocity-changing collisions are randomly distributed. Therefore, the whole Doppler profile will, in general, not be affected and the effect of these collisions is canceled out in Doppler-limited spectroscopy. In Doppler-free laser spectroscopy, however, the velocity-changing collisions may play a non-negligible role. They cause effects that depend on the ratio of the mean time $T = \Lambda/\overline{v}$ between collisions to the interaction time $\tau_c$ with the radiation field. For $T > \tau_c$, the redistribution of molecules by velocity-changing collisions causes only a small change of the population densities $n_i(v_z)\,\mathrm{d}v_z$ within the different subgroups, without noticeably changing the homogeneous width of this subgroup. If $T \ll \tau_c$, the different subgroups are uniformly mixed. This results in a broadening of the homogeneous linewidth associated with each subgroup. The effective interaction time of the molecules with a monochromatic laser field is shortened because the velocity-changing collisions move a molecule out of resonance with the field. The resultant change of the line shape can be monitored using saturation spectroscopy (Vol. 2, Sect. 2.3).

Under certain conditions, if the mean free path $\Lambda$ of the molecules is smaller than the wavelength of the radiation field, velocity-changing collisions may also result in a narrowing of a Doppler-broadening line profile (Dicke narrowing, Sect. 3.3.3).

## 3.6 Saturation and Power Broadening

At sufficiently large laser intensities, the optical pumping rate on an absorbing transition becomes larger than the relaxation rates. This results in a noticeable decrease of the population in the absorbing levels. This saturation of the population densities also causes additional line broadening. The spectral line profiles of such partially saturated transitions are different for homogeneously and for inhomogeneously broadened lines [3.39]. Here we treat the homogeneous case, while the saturation of inhomogeneous line profiles is discussed in Vol. 2, Chap. 2.

### 3.6.1 Saturation of Level Population by Optical Pumping

The effect of optical pumping on the saturation of population densities is illustrated by a two-level system with population densities $N_1$ and $N_2$. The two levels are coupled to each other by absorption or emission and by relaxation processes, but have no transitions to other levels (Fig. 3.22). Such a "true" two-level system is realized by many atomic resonance transitions without hyperfine structure.

With the probability $\mathfrak{P}_{12} = B_{12}\rho(\omega)$ for a transition $|1\rangle \rightarrow |2\rangle$ by absorption of photons $\hbar\omega$ and the relaxation probability $R_i$ for level $|i\rangle$, the rate equation for the level population is

$$\frac{\mathrm{d}N_1}{\mathrm{d}t} = -\frac{\mathrm{d}N_2}{\mathrm{d}t} = -\mathfrak{P}_{12}N_1 - R_1N_1 + \mathfrak{P}_{12}N_2 + R_2N_2 \,, \tag{3.66}$$

where we have assumed nondegenerate levels with statistical weight factors $g_1 = g_2 = 1$. Under stationary conditions ($\mathrm{d}N_i/\mathrm{d}t = 0$) we obtain with $N_1 + N_2 = N$ from (3.66) with the abbreviation $\mathfrak{P}_{12} = P$

$$(P + R_1)N_1 = (P + R_2)(N - N_1) \;\Rightarrow\; N_1 = N\frac{P + R_2}{2P + R_1 + R_2} \tag{3.67a}$$

$$(P + R_2)N_2 = (P + R_1)(N - N_2) \;\Rightarrow\; N_2 = N\frac{P + R_1}{2P + R_1 + R_2} \,. \tag{3.67b}$$

When the pump rate $P$ becomes much larger than the relaxation rates $R_i$, the population $N_1$ approaches $N/2$, i.e., $N_1 = N_2$. This means that the absorption coefficient $\alpha = \sigma(N_1 - N_2)$ goes to zero (Fig. 3.23). The medium becomes completely transparent.

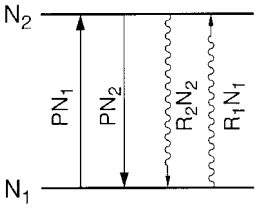


**Fig. 3.22.** Two-level system with no relaxation into other levels

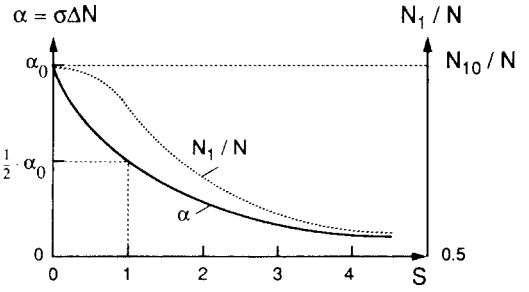


**Fig. 3.23.** Saturation of population density $N_1$ and absorption coefficient $\alpha = \sigma(N_1 - N_2)$ as functions of the saturation parameter $S$ (see text)

Without a radiation field ($P = 0$), the population densities at thermal equilibrium according to (3.67) are

$$N_{10} = \frac{R_2}{R_1 + R_2} N \; ; \quad N_{20} = \frac{R_1}{R_1 + R_2} N \; . \tag{3.67c}$$

With the abbreviations

$$\Delta N = N_1 - N_2 \quad \text{and} \quad \Delta N_0 = N_{10} - N_{20}$$

we obtain from (3.67) and (3.67c)

$$\Delta N = N \frac{R_2 - R_1}{2P + R_1 + R_2}$$
$$\Delta N_0 = N \frac{R_2 - R_1}{R_2 + R_1}$$

which gives:

$$\Delta N = \frac{\Delta N_0}{1 + 2P/(R_1 + R_2)} = \frac{\Delta N_0}{1 + S} \; . \tag{3.67d}$$

The *saturation parameter*

$$S = 2P/(R_1 + R_2) = P/\overline{R} = B_{12}\rho(\omega)/\overline{R} \tag{3.67e}$$

represents the ratio of pumping rate $P$ to the average relaxation rate $\overline{R} = (R_1 + R_2)/2$. If the spontaneous emission of the upper level $|2\rangle$ is the only relaxation mechanism, we have $R_1 = 0$ and $R_2 = A_{21}$. Since the pump rate due to a monochromatic wave with intensity $I(\omega)$ is $P = \sigma_{12}(\omega) I(\omega)/\hbar\omega$, we obtain for the saturation parameter

$$S = \frac{2\sigma_{12} I(\omega)}{\hbar\omega A_{12}} \; . \tag{3.67f}$$

The saturated absorption coefficient $\alpha(\omega) = \sigma_{12}\Delta N$ is, according to (3.67d),

$$\boxed{\alpha = \frac{\alpha_0}{1 + S} \; ,} \tag{3.68}$$

where $\alpha_0$ is the unsaturated absorption coefficient without pumping.

### 3.6.2 Saturation Broadening of Homogeneous Line Profiles

According to (2.15) and (3.67d), the power absorbed per unit volume on the transition $|1\rangle \rightarrow |2\rangle$ by atoms with the population densities $N_1$, $N_2$ in a radiation field with a broad spectral profile and spectral energy density $\rho$ is

$$\frac{\mathrm{d}W_{12}}{\mathrm{d}t} = \hbar\omega B_{12}\rho(\omega)\Delta N = \hbar\omega B_{12}\rho(\omega)\frac{\Delta N_0}{1+S} \,. \tag{3.69}$$

With $S = B_{12}\rho(\omega)/\overline{R}$, see (3.67e), this can be written as

$$\frac{\mathrm{d}W_{12}}{\mathrm{d}t} = \hbar\omega\overline{R}\frac{\Delta N_0}{1+S^{-1}} \,. \tag{3.70}$$

Since the absorption profile $\alpha(\omega)$ of a homogeneously broadened line is Lorentzian, see (3.36b), the induced absorption probability of a monochromatic wave with frequency $\omega$ follows a Lorentzian line profile $B_{12}\rho(\omega) \cdot L(\omega-\omega_0)$. We can therefore introduce a frequency-dependent spectral saturation parameter $S_\omega$ for the transition $E_1 \rightarrow E_2$,

$$S_\omega = \frac{B_{12}\rho(\omega)}{\overline{R}} L(\omega-\omega_0) \,. \tag{3.71}$$

We can assume that the mean relaxation rate $\overline{R}$ is independent of $\omega$ within the frequency range of the line profile. With the definition (3.36b) of the Lorentzian profile $L(\omega-\omega_0)$, we obtain for the spectral saturation parameter $S_\omega$

$$S_\omega = S_0\frac{(\gamma/2)^2}{(\omega-\omega_0)^2+(\gamma/2)^2} \quad \text{with} \quad S_0 = S_\omega(\omega_0) \,. \tag{3.72}$$

Substituting (3.72) into (3.70) yields the frequency dependence of the absorbed radiation power per unit frequency interval $\mathrm{d}\omega = 1\,\mathrm{s}^{-1}$

$$\frac{\mathrm{d}}{\mathrm{d}t}W_{12}(\omega) = \frac{\hbar\omega\overline{R}\Delta N_0 S_0(\gamma/2)^2}{(\omega-\omega_0)^2+(\gamma/2)^2(1+S_0)} = \frac{C}{(\omega-\omega_0)^2+(\gamma_\mathrm{s}/2)^2} \,. \tag{3.73}$$

This a Lorentzian profile with the increased halfwidth

$$\gamma_\mathrm{s} = \gamma\sqrt{1+S_0} \,. \tag{3.74}$$

The halfwidth $\gamma_\mathrm{s} = \delta\omega_\mathrm{s}$ of the saturation-broadened line increases with the saturation parameter $S_0$ at the line center $\omega_0$. If the induced transition rate at $\omega_0$ equals the total relaxation rate $\overline{R}$, the saturation parameter $S_0 = [B_{12}\rho(\omega_0)]/\overline{R}$ becomes $S_0 = 1$, which increases the linewidth by a factor $\sqrt{2}$, compared to the unsaturated linewidth $\delta\omega_0$ for weak radiation fields ($\rho \rightarrow 0$).

Since the power $\mathrm{d}W_{12}/\mathrm{d}t$ absorbed per unit volume equals the intensity decrease per centimeter, $\mathrm{d}I = -\alpha_\mathrm{s} I$, of an incident wave with intensity $I$, we

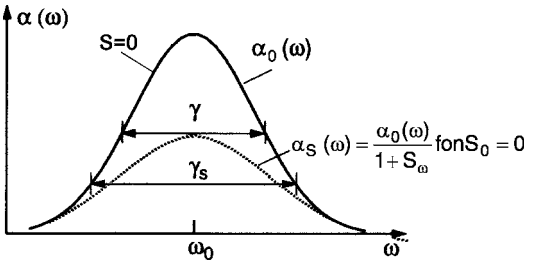


**Fig. 3.24.** Saturation broadening of a homogeneous line profile

can derive the absorption coefficient $\alpha$ from (3.73). With $I = c\rho$ and $S_\omega$ from (3.72) we obtain

$$\alpha_s(\omega) = \alpha_0(\omega_0)\frac{(\gamma/2)^2}{(\omega-\omega_0)^2+(\gamma_s/2)^2} = \frac{\alpha_0(\omega)}{1+S_\omega}\,, \tag{3.75}$$

where the unsaturated absorption profile is

$$\alpha_0(\omega) = \frac{\alpha_0(\omega_0)(\gamma/2)^2}{(\omega-\omega_0)^2+(\gamma/2)^2} \tag{3.76}$$

with $\alpha_0(\omega_0) = 2\hbar\omega B_{12}\Delta N_0/\pi c\gamma$.

This shows that the saturation decreases the absorption coefficient $\alpha(\omega)$ by the factor $(1+S_\omega)$. At the line center, this factor has its maximum value $(1+S_0)$, while it decreases for increasing $(\omega-\omega_0)$ to 1, see (3.72). The saturation is therefore strongest at the line center, and approaches zero for $(\omega-\omega_0)\to\infty$ (Fig. 3.24). This is the reason why the line broadens. For a more detailed discussion of saturation broadening, see Vol. 2, Chap. 2 and [3.38–3.40].

### 3.6.3 Power Broadening

The broadening of homogeneous line profiles by intense laser fields can also be regarded from another viewpoint compared to Sect. 3.6.2. When a two-level system is exposed to a radiation field $E = E_0\cos\omega t$, the population probability of the upper level $|b\rangle$ is, according to (2.67) and (2.89),

$$|b(\omega,t)|^2 = \frac{D_{ab}^2E_0^2}{\hbar^2(\omega_{ab}-\omega)^2+D_{ab}^2E_0^2} \times \sin^2\left[\frac{1}{2}\sqrt{(\omega_{ab}-\omega)^2+(D_{ab}E_0/\hbar)^2}\cdot t\right], \tag{3.77}$$

an oscillatory function of time, which oscillates at exact resonance $\omega = \omega_{ab}$ with the Rabi flopping frequency $\Omega_R = \Omega_{ab} = D_{ab}E_0/\hbar$.

If the upper level $|b\rangle$ can decay by spontaneous processes with a relaxation constant $\gamma$, its mean population probability is

$$\mathcal{P}_b(\omega) = \overline{|b(\omega, t)|}^2 = \int_0^\infty \gamma \, \mathrm{e}^{-\gamma t} \, |b(\omega_1, t)|^2 \, \mathrm{d}t \, . \tag{3.78}$$

Inserting (3.77) and integrating yields

$$\mathcal{P}_b(\omega) = \frac{1}{2} \frac{D_{ab}^2 E_0^2/\hbar^2}{(\omega_{ab} - \omega)^2 + \gamma^2(1+S)} \, , \tag{3.79}$$

with $S = D_{ab}^2 E_0^2/(\hbar^2\gamma^2)$. Since $\mathcal{P}_b(\omega)$ is proportional to the absorption line profile, we obtain as in (3.73) a power-broadened Lorentzian line profile with the linewidth

$$\gamma_S = \gamma\sqrt{1+S} \, .$$

Since the induced absorption rate within the spectral interval $\gamma$ is, according to (2.41) and (2.77)

$$B_{12}\rho\gamma = B_{12} I\gamma/c \simeq D_{12}^2 E_0^2/\hbar^2 \, , \tag{3.80}$$

the quantity $S$ in (3.79) turns out to be identical with the saturation parameter $S$ in (3.67e).

If both levels $|a\rangle$ and $|b\rangle$ decay with the relaxation constants $\gamma_a$ and $\gamma_b$, respectively, the line profile of the homogeneously broadened transition $|a\rangle \rightarrow |b\rangle$ is again described by (3.79), where now (Vol. 2, Sect. 2.1 and [3.40])

$$\gamma = \tfrac{1}{2}(\gamma_a + \gamma_b) \quad \text{and} \quad S = D_{ab}^2 E_0^2/(\hbar^2\gamma_a\gamma_b) \, . \tag{3.81}$$

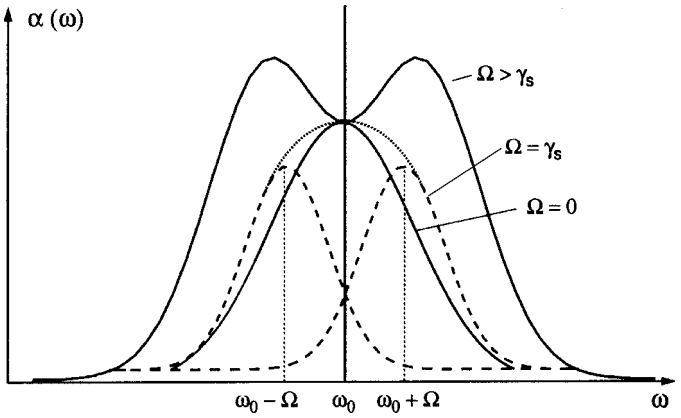


**Fig. 3.25.** Absorption profile of a homogeneous transition pumped by a strong pump wave kept at $\omega_0$ and probed by a weak tunable probe wave for different values of the ratio $\Omega/\gamma_S$ of the Rabi frequency $\Omega$ to the linewidth $\gamma_S$

If a strong pump wave is tuned to the center $\omega_0 = \omega_{ab}$ of the transition and the absorption profile is probed by a tunable weak probe wave, the absorption profile looks different: due to the population modulation with the Rabi flopping frequency $\Omega$, sidebands are generated at $\omega_0 \pm \Omega$ that have the homogeneous linewidth $\gamma_S$. The superposition of these sidebands (Fig. 3.25) gives a line profile that depends on the ratio $\Omega/\gamma_S$ of the Rabi flopping frequency $\Omega$ and the saturated linewidth $\gamma_S$. For a sufficiently strong pump wave ($\Omega > \gamma_S$), the separation of the sidebands becomes larger than their width and a dip appears at the center $\omega_0$.

## 3.7 Spectral Line Profiles in Liquids and Solids

Many different types of lasers use liquids or solids as amplifying media. Since the spectral characteristics of such lasers play a significant role in applications of laser spectroscopy, we briefly outline the spectral linewidths of optical transitions in liquids and solids. Because of the large densities compared with the gaseous state, the mean relative distances $R(\mathrm{A}, \mathrm{B}_j)$ between an atom or molecule A and its surrounding partners $\mathrm{B}_j$ are very small (typically a few tenths of a nanometer), and the interaction between A and the adjacent partners $\mathrm{B}_j$ is accordingly large.

In general, the atoms or molecules used for laser action are diluted to small concentrations in liquids or solids. Examples are the dye laser, where dye molecules are dissolved in organic solutions at concentrations of $10^{-4}$ to $10^{-3}$ moles/liter, or the ruby laser, where the relative concentration of the active $Cr^{3+}$ ions in $Al_3O_3$ is on the order of $10^{-3}$. The optically pumped laser molecules $\mathrm{A}^*$ interact with their surrounding host molecules B. The resulting broadening of the excited levels of $\mathrm{A}^*$ depends on the total electric field produced at the location of A by all adjacent molecules $\mathrm{B}_j$, and on the dipole moment or the polarizability of $\mathrm{A}^*$. The linewidth $\Delta\omega_{ik}$ of a transition $A^*(E_i) \rightarrow A^*(E_k)$ is determined by the difference in the level shifts $(\Delta E_i - \Delta E_k)$.

In liquids, the distances $R_j(\mathrm{A}^*, \mathrm{B}_j)$ show random fluctuations analogous to the situation in a high-pressure gas. The linewidth $\Delta\omega_{ik}$ is therefore determined by the probability distribution $P(R_j)$ of the mutal distances $R_j(\mathrm{A}^*, \mathrm{B}_j)$ and the correlation between the phase perturbations at $\mathrm{A}^*$ caused by elastic collisions during the lifetime of the levels $E_i$, $E_k$ (see the analogous discussion in Sect. 3.3).

Inelastic collisions of $\mathrm{A}^*$ with molecules B of the liquid host may cause radiationless transitions from the level $E_i$ populated by optical pumping to lower levels $E_n$. These radiationless transitions shorten the lifetime of $E_i$ and cause collisional line broadening. In liquids the mean time between successive inelastic collisions is of the order of $10^{-11}$ to $10^{-13}$ s. Therefore the spectral line $E_i \rightarrow E_k$ is greatly broadened with a homogeneously broadened profile. When the line broadening becomes larger than the separation of the different spectral lines, a broad continuum arises. In the case of molecular spectra